

# Paper B

## Ligand Noninnocence

## Ligand Noninnocence in Iron Corroles: Insights from Optical and X-ray Absorption Spectroscopies and Electrochemical Redox Potentials

Sumit Ganguly,<sup>[a]</sup> Logan J. Giles,<sup>[b]</sup> Kolle E. Thomas,<sup>[a]</sup> Ritimukta Sarangi,<sup>\*[b]</sup> and Abhik Ghosh<sup>\*[a]</sup>

**Abstract:** Two new series of iron *meso*-tris(*para*-X-phenyl)-corrole (TpXPC) complexes, Fe[TpXPC]Ph and Fe[TpXPC]Tol, in which X = CF<sub>3</sub>, H, Me, and OMe, and Tol = *p*-methylphenyl (*p*-tolyl), have been synthesized, allowing a multitechnique electronic–structural comparison with the corresponding FeCl, FeNO, and Fe<sub>2</sub>( $\mu$ -O) TpXPC derivatives. Optical spectroscopy revealed that the Soret maxima of the FePh and FeTol series are insensitive to the phenyl *para* substituent, consistent with the presumed innocence of the corrole ligand in these compounds. Accordingly, we may be increasingly confident in the ability of the substituent effect criterion to serve as a probe of corrole noninnocence. Furthermore, four complexes—Fe[TPC]Cl, Fe[TPC](NO), {Fe[TPC]}<sub>2</sub>O, and Fe[TPC]Ph—were selected for a detailed XANES investigation of the question of ligand noninnocence. The intensity-

weighted average energy (IWAE) positions were found to exhibit rather modest variations (0.8 eV over the series of corroles). The integrated Fe-K pre-edge intensities, on the other hand, vary considerably, with a 2.5 fold increase for Fe[TPC]Ph relative to Fe[TPC]Cl and Fe[TPC](NO). Given the approximately C<sub>4v</sub> local symmetry of the Fe in all the complexes, the large increase in intensity for Fe[TPC]Ph may be attributed to a higher number of 3d holes, consistent with an expected Fe<sup>IV</sup>-like description, in contrast to Fe[TPC]Cl and Fe[TPC](NO), in which the Fe is thought to be Fe<sup>III</sup>-like. These results afford strong validation of XANES as a probe of ligand noninnocence in metallocorroles. Electrochemical redox potentials, on the other hand, were found not to afford a simple probe of ligand noninnocence in Fe corroles.

## Introduction

Metallocorroles have emerged as new paradigms for the phenomenon of ligand noninnocence.<sup>[1]</sup> The phenomenon is especially common among first-row transition metal corroles, particularly Mn,<sup>[2]</sup> Fe, and Cu<sup>[3]</sup> corroles, but is also known for other metallocorroles. Early on, NMR spectroscopy and DFT calculations established that whereas FeCl corroles are noninnocent, that is, best represented as Fe<sup>III</sup>-corrole<sup>2-</sup>, Fe  $\sigma$ -aryl corroles are essentially innocent, that is, Fe<sup>IV</sup>-corrole<sup>3-</sup>.<sup>[4–7]</sup> Ligand noninnocence in Fe corroles arises through an Fe(d<sub>22</sub>)-corrole( $\pi$ ) orbital interaction, which, understandably, is strongly affected by the nature of the axial ligand.<sup>[8]</sup> In contrast, EPR spec-


troscopy and DFT calculations have shown that Pt  $\sigma$ -diaryl derivatives Pt[Cor]ArAr' are best viewed as *full-fledged* corrole radicals, that is, Pt<sup>IV</sup>-corrole<sup>2-</sup>.<sup>[9]</sup>

NMR and EPR spectroscopy, however, are of little use for probing the potential noninnocence of diamagnetic metallocorroles, in which putative corrole<sup>2-</sup> radicals are more cryptic as a result of antiferromagnetic coupling to a metal center, which leads to an overall diamagnetic ground state. Copper corroles provide some of the most striking examples of such cryptic noninnocence.<sup>[3]</sup> Spin coupling between the corrole a<sub>2u</sub>-type radical (for which, out of convention, we have used the porphyrin D<sub>4h</sub> irreducible representation) and the Cu3d<sub>x<sup>2</sup>-y<sup>2</sup></sub> electron results in a marked saddling of the corrole macrocycle. Such strong saddling is not observed for gold corroles owing to an energy mismatch between the Au5d<sub>x<sup>2</sup>-y<sup>2</sup></sub> orbital and the corrole a<sub>2u</sub> HOMO; Au corroles thus are best viewed as Au<sup>III</sup>-corrole<sup>3-</sup>.<sup>[10]</sup> Recently, we showed that FeNO<sup>[11]</sup> corroles and  $\mu$ -oxo di-iron<sup>[12]</sup> corroles provide additional examples of cryptic noninnocence, that is, of diamagnetic metallocorroles that are nonetheless best thought of as corrole<sup>2-</sup> radical derivatives.

For *meso*-tris(*para*-X-phenyl)corrole (TpXPC) complexes (Figure 1), the optical spectra provide a simple, empirical probe of ligand noninnocence. For noninnocent metallotriarylcorroles, increasingly electron-donating *para* substituents X

[a] S. Ganguly, K. E. Thomas, Prof. Dr. A. Ghosh  
Department of Chemistry and Center  
for Theoretical and Computational Chemistry  
UiT-The Arctic University of Norway, 9037 Tromsø (Norway)  
E-mail: abhik.ghosh@uit.no

[b] Dr. L. J. Giles, Dr. R. Sarangi  
Structural Molecular Biology  
Stanford Synchrotron Radiation Lightsource  
SLAC National Accelerator Laboratory  
Menlo Park, CA, 94306 (USA)  
E-mail: ritis@slac.stanford.edu

 The ORCID identification number(s) for the author(s) of this article can be found under <https://doi.org/10.1002/chem.201702621>.

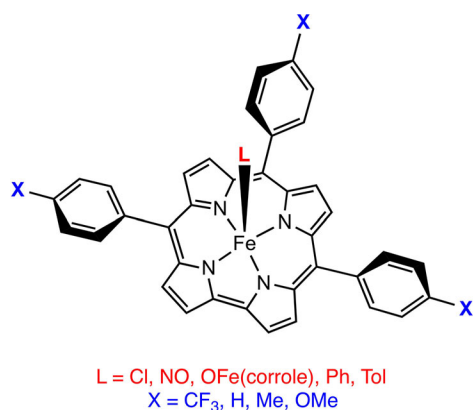


Figure 1. Complexes studied in this work.

lead to systematic redshifts in the Soret maxima.<sup>[2a-4,9,11,12]</sup> The substituent-sensitive component of the Soret manifold in these cases is thought to be an aryl $\rightarrow$ corrole<sup>2-</sup> charge-transfer transition.<sup>[13,14]</sup> No analogous spectral shifts are observed for innocent metallotriarylcorroles.<sup>[10,15-18]</sup> This empirical correlation has proven so reliable that we used it in a predictive manner to identify new families of noninnocent complexes, notably FeNO<sup>[11]</sup> corroles and  $\mu$ -oxo di-iron<sup>[12]</sup> corroles.

In this study, we have examined critically the insight afforded by three lines of evidence, namely Fe K-edge X-ray absorption spectra and associated optical spectra, and electrochemical redox potentials. Given the sensitivity of the pertinent  $1s \rightarrow 3d$  pre-edge of the X-ray absorption spectra of transition metals to d electron counts,<sup>[19]</sup> it is remarkable that XAS has rarely been applied to metallocorroles.<sup>[20]</sup> Presented herein are the K-edge X-ray absorption near-edge spectroscopy (XANES) data on Fe[TPC]Cl, Fe[TPC](NO){Fe[TPC]}<sub>2</sub>O, and Fe[TPC]Ph, allowing a critical examination of the method as a probe of ligand noninnocence in Fe corroles. A reasonable amount of information is already available on the optical spectra of FeCl, FeNO, and Fe<sub>2</sub>( $\mu$ -O) TpXPC derivatives. Analogous substituent effect data on Fe[TpXPC]Ar derivatives, however, have not been reported until now. Two new series of Fe corroles were synthesized in this study, namely, Fe[TpXPC]Ph and Fe[TpXPC]-Tol, in which X=CF<sub>3</sub>, H, Me, and OMe, and Tol=*p*-methylphenyl (tolyl), enabling us to apply the aforementioned optical probe to test the innocence or otherwise of these complexes. The new series of Fe corroles also permitted us to undertake an electrochemical study,<sup>[21]</sup> where we sought to determine whether the redox potentials might afford a simple probe of the innocence or noninnocence of metallocorroles. To that end, we also re-examined the redox potentials of the FeCl, FeNO, and Fe<sub>2</sub>( $\mu$ -O) TpXPC derivatives. Overall, we sought to evaluate how the evidence afforded by XANES with respect to ligand noninnocence might dovetail with that afforded by other methods such as optical spectroscopy, electrochemistry, and DFT calculations.

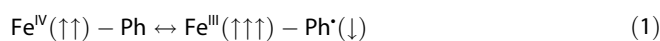
## Results and Discussion

### The optical probe applied to Fe[TpXPC]Ar (Ar = Ph, Tol)

Figure 2 depicts the optical spectra of the two new series Fe[TpXPC]Ar (Ar=Ph, Tol), along with those of the previously reported FeCl, FeNO, and Fe<sub>2</sub>( $\mu$ -O) series, which were also re-determined in this study for accuracy and completeness. Table 1 lists the Soret maxima of all the complexes. The results clearly show that the Soret maxima of the two Fe-aryl series are essentially invariant with respect to the *para* substituent X, confirming the consensus view that the corrole ligands in these complexes are expected to be innocent.<sup>[1,5,6]</sup> An interesting point here is that the substituent effects on the Soret maxima are considerably higher for the FeCl and FeNO series than they are for the Fe<sub>2</sub>( $\mu$ -O) series, which leads to the question of whether these differences might signify differences in the degree of corrole radical character among the three noninnocent series of complexes.<sup>[22]</sup>

DFT calculations have long indicated an essentially innocent corrole ligand for Fe[TPC]Ph.<sup>[1,5]</sup> In a first approximation, no substantial spin populations were found to reside on the corrole ligand.<sup>[11,5,23]</sup> The <sup>1</sup>H NMR spectra (Table 2) also evince no indication of an "a<sub>2u</sub>-type" corrole radical, which would have led to significant paramagnetic shifts for *meso*-aryl protons.<sup>[24]</sup> Careful examination of the DFT spin density profile does, however, reveal small excess spin populations at certain carbon atoms, including the  $\beta$ -carbons C<sub>3/17</sub> and C<sub>8/12</sub> and the *ortho* and *para* carbons of the axial phenyl group. These also happen to be the positions at which the attached protons exhibit the largest paramagnetic shifts (Table 2), which strongly suggests that the DFT spin density profile provides a relatively accurate representation of reality.

The only carbon atom with a fairly large Mulliken spin population is the *ipso* carbon of the  $\sigma$ -aryl group, which, in B3LYP calculations, carries a minority spin population of around -0.15. That, along with the fact that the Fe carries a majority spin population greater than approximately 2.0, appears to be indicative of a certain amount of intermediate-spin Fe<sup>III</sup> character, as shown in Equation (1).



The exact point at which a given Fe-aryl corrole lies on this continuum can potentially be determined through advanced multiconfigurational *ab initio* calculations;<sup>[25]</sup> such studies, however, have not been undertaken at this point.

### XANES analysis

Four compounds, Fe[TPC]Cl, Fe[TPC](NO), {Fe[TPC]}<sub>2</sub>O, and Fe[TPC]Ph, were selected for an Fe K-edge XAS investigation of higher-valent Fe corroles (Figure 3). The Fe K pre-edge region is a sensitive probe of the electronic and geometric structure, and reflects an excitation of the Fe 1s core electron to the valence molecular orbitals with Fe 3d character. This  $1s \rightarrow 3d$  excitation is electric-dipole forbidden but electric-quadrupole al-

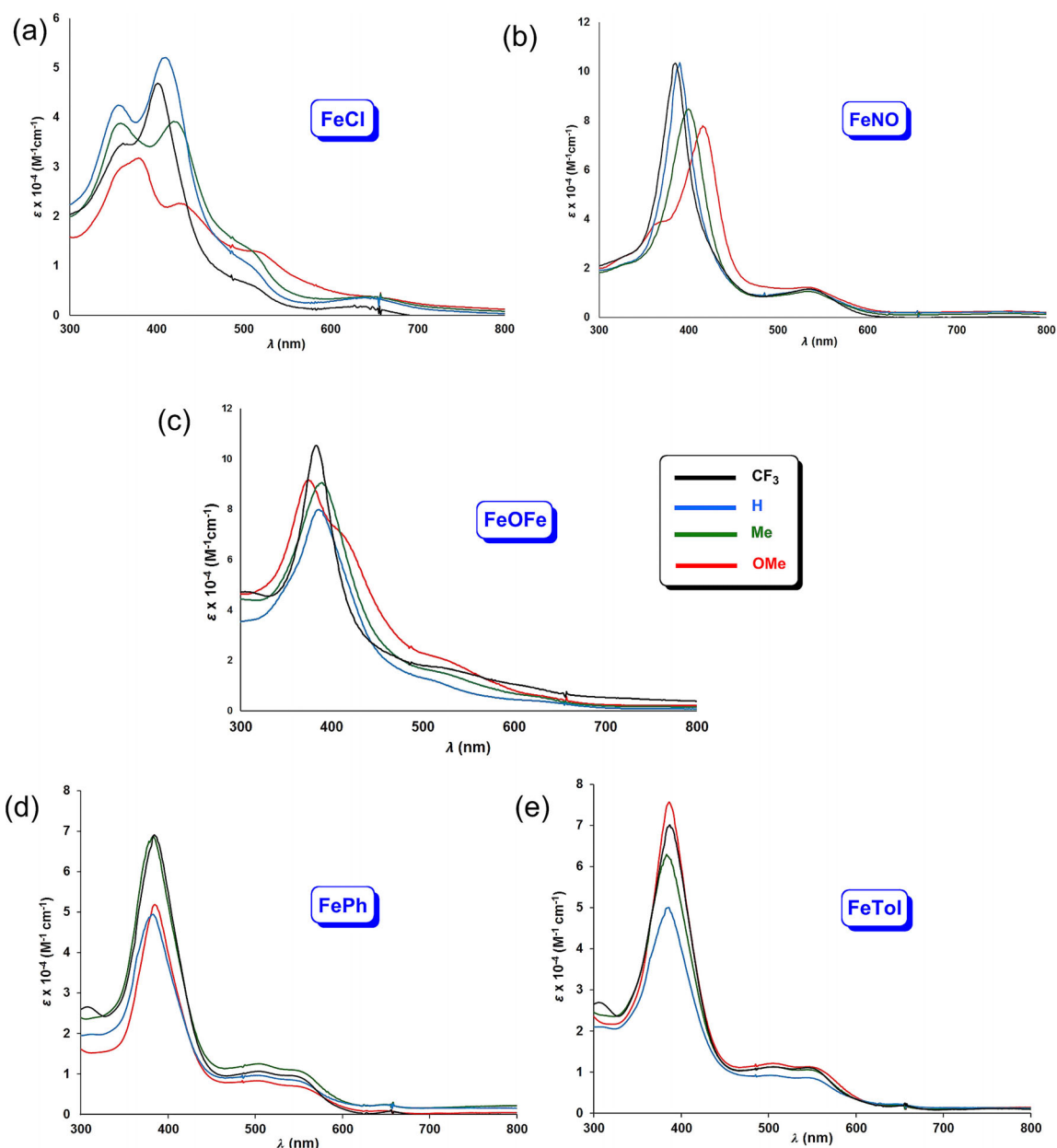


Figure 2. UV/Vis spectra of Fe corroles in dichloromethane.

lowed, and gains intensity through symmetry-allowed metal 3d–4p mixing. The XANES data revealed significant differences between the four compounds in the pre-edge energy position and intensities. Previous studies have shown that the pre-edge

**Table 1.** Soret maxima (nm) of different tris(*p*-X-phenyl)corrole derivatives.

Series	<i>para</i> substituent X			
	CF <sub>3</sub>	H	Me	OMe
Fe[TpXPC]Cl	401	410	419	426
Fe[TpXPC](NO)	385	390	400	416
{Fe[TpXPC]} <sub>2</sub> (μ-O)	383	386	389	375, 410
Fe[TpXPC]Ph	384	383	383	385
Fe[TpXPC]Tol	387	385	383	386

energy is influenced strongly by the ligand field, shifting to higher energies with an increase in ligand field strength. The intensity weighted average energy (IWAE) positions exhibit the following order: Fe[TPC]Cl (7113.2 eV) < Fe[TPC](NO) (7113.5 eV) < Fe[TPC]Ph (7113.8) < {[Fe[TPC]}<sub>2</sub>O} (7114 eV). Superficially, this ordering appears to be consistent with an increase in ligand field strength on going from Fe[TPC]Cl to {[Fe[TPC]}<sub>2</sub>O}. Note, however, that the energy shifts in the pre-edges are relatively small, as the largest contributor to the ligand field is the TPC ligand, which is the same in all four systems. The integrated pre-edge intensities, however, show a more dramatic trend and follow the order: Fe[TPC]Cl (1.37) < Fe[TPC](NO) (1.55) < {[Fe[TPC]}<sub>2</sub>O} (3.02) < Fe[TPC]Ph (3.61). Thus, the intensity of Fe[TPC]Ph is approximately 2.5 times that of Fe[TPC]Cl.

Series	2,18- $\beta$	3,17- $\beta$	7,13- $\beta$	8,12- $\beta$	5,15-o	5,15-m	5,15-p	10-o	10-m	10-p	$\sigma$ -Ar-o	$\sigma$ -Ar-m	$\sigma$ -Ar-p
Fe[TpCF <sub>3</sub> PC]Ph	-31.15	-110.6	12.08-11.50	-59.05	14.59, 13.56	6.66, 6.43	-	12.08-11.50	6.18,6.07	-	-163.10	-3.41	-89.80
Fe[TPC]Ph	-30.90	-109.66	10.95	-56.74	13.79	6.26, 6.02	10.86	11.98, 11.83	5.72,5.6	9.65	-155.89	0.51	-87.41
Fe[TpMePC]Ph <sup>[a]</sup>	-30.7	-109.1	10.5	-55.9	14.8, 13.8	6.0, 5.7	0.8 (pMe)	12.0, 11.9	5.4, 5.2	0.6 (pMe)	-154.0	0.3	-86.7
Fe[TpOMePC]Ph	-30.73	-108.98	10.23	-55.23	14.89, 13.81	5.88, 5.61	4.17 (pOMe)	12.17, 11.97	5.22,5.07	3.92 (pOMe)	-153.07	0.66	-86.48
Fe[TpCF <sub>3</sub> PC]Tol	-30.24	-114.20	12.01-11.19	-57.33	14.51, 13.45	6.69, 6.45	-	12.01-11.19	6.25, 6.14	-	-165.23	0.25	-107.72
Fe[TPC]Tol	-30.00	-152.46	10.71	-55.26	14.73, 13.7	6.27, 6.04	10.81	11.94, 11.77	5.77,5.64	9.62	-158.69	2.89	-107.22 (pMe)
Fe[TpMePC]Tol	-29.97	-156.81	10.30	-54.57	14.75, 13.7	5.97, 5.73	0.62 (pMe)	12.0, 11.79	5.41,5.27	0.82 (pMe)	-162.99	3.58	-106.93 (pMe)
Fe[TpOMePC]Tol	-29.87	-118.06	10.02	-53.83	14.82, 13.72	5.89, 5.62	4.17 (pOMe)	12.13, 11.91	5.30,5.11	3.93 (pOMe)	-155.61	br	-106.58 (pMe)

[a] These values are obtained from Ref. [7].

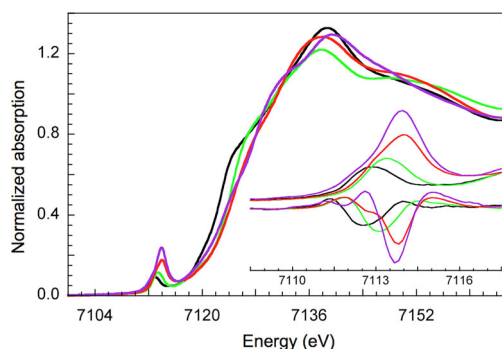
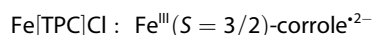


**Figure 3.** Normalized Fe K-edge XANES data for Fe[TPC]Cl (black), Fe[TPC](-NO) (green), {Fe[TPC]}<sub>2</sub>O (red), and Fe[TPC]Ph (purple). The inset displays the pre-edge region (bottom) and the corresponding first derivative (top).

Two mechanisms are available for an increase in Fe K pre-edge intensity: 1) an increase in the number of available metal 3d holes (associated with oxidation at the Fe center), and 2) an increase in metal 3d-4p mixing (associated with a decrease in centrosymmetry). Typically, the metal 3d-4p mixing contribution is the dominant factor (quadrupole-only transitions are  $\approx 1\%$  of a dipole-only transition). However, both these factors may act synergistically if the additional 3d hole caused by an increase in Fe oxidation state can also participate in symmetry-allowed 3d-4p mixing. All four complexes examined here exhibit similar square-pyramidal geometries, with the axial ligand providing the key difference. This similarity allows a systematic comparison of the complexes and elucidation of the factors responsible for the aforementioned dramatic change in pre-edge intensity. To this end, we performed a detailed TDDFT study of the Fe K pre-edge spectra of Fe[TPC]Cl and Fe[TPC]Ph. These two complexes were chosen for two reasons: 1) they exhibit the biggest difference in both their Fe K pre-edge energies and integrated intensities, and 2) they are both  $S=1$  systems, whereas Fe[TPC](NO) and {Fe[TPC]}<sub>2</sub>O are both open-shell singlets involving more than two open-shell centers in their broken symmetry descriptions. As expected, the ground-state

Mulliken spin densities of the two complexes examined were consistent with the following ground state descriptions:<sup>[1,5]</sup>



and

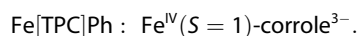
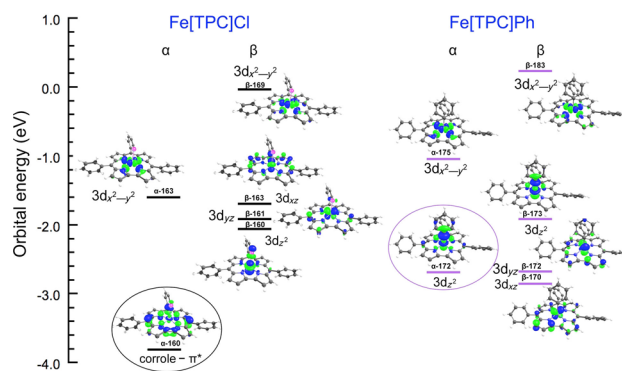
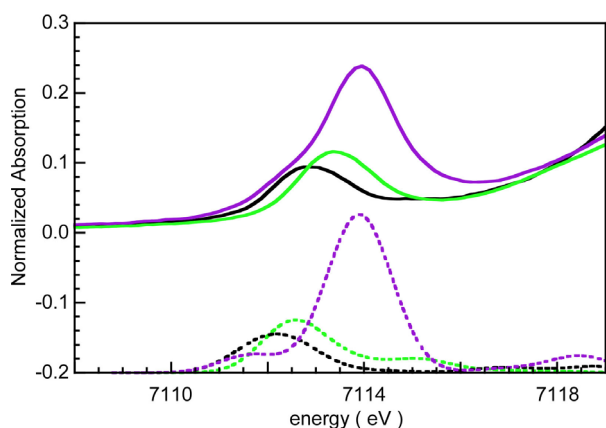


Figure 4 depicts the energy levels and contour plots of the unoccupied Fe 3d-based valence MOs relevant to the Fe K pre-edges. In the spin-unrestricted formalism, the Fe<sup>III</sup>( $S=3/2$ )-corrole<sup>2-</sup> and Fe<sup>IV</sup>( $S=1$ )-corrole<sup>3-</sup> configurations differ in the composition of the majority-spin ( $\alpha$ ) LUMO. For Fe<sup>III</sup>( $S=3/2$ )-corrole<sup>2-</sup>, the  $\alpha$ -LUMO should be predominantly corrole-based, whereas for Fe<sup>IV</sup>( $S=1$ )-corrole<sup>3-</sup> it should be Fe-based. This is exactly what is found for the  $\alpha$ -LUMOs of Fe[TPC]Cl and Fe[TPC]Ph (circled and highlighted in Figure 4). Furthermore, the metal-based  $\alpha$ -LUMO is an Fe3d<sub>z<sup>2</sup></sub> orbital with potential for 3d<sub>z<sup>2</sup></sub>-4p<sub>z</sub> mixing. As shown in Figure 5, the calculated TDDFT spectra of Fe[TPC]Cl, Fe[TPC](NO), and Fe[TPC]Ph were found to be in reasonably good agreement with the experimental



**Figure 4.** Lowest unoccupied MO energy levels and contour plots for Fe[TPC]Cl and Fe[TPC]Ph. Only the Fe 3d-based MOs are shown, and ligand-based MOs have been omitted for clarity.



**Figure 5.** Comparison of the TDDFT calculated  $1s \rightarrow 3d$  spectra (dotted lines) with the experimental data (solid lines) for Fe[TPC]Cl (black), Fe[TPC](NO) (green), and Fe[TPC]Ph (purple).

data and reproduced the dramatic differences in pre-edge intensities. TDDFT results on  $\{\text{Fe}[\text{TPC}]\}_2\text{O}$  are not included in Figure 5, because the calculations on the larger molecule could only be performed with a smaller basis set.

Figure 6 depicts the individual transitions contributing to the calculated  $1s \rightarrow 3d$  envelopes of Fe[TPC]Cl and Fe[TPC]Ph, along with their MO origins and electric dipole and quadrupole contributions. Evidently, the electric dipole contributions are by far the more dominant. For Fe[TPC]Cl, three states account for the majority of the calculated pre-edge intensity. Of these, States 1 and 2 approximately overlap at 6961.1 eV, whereas State 3 occurs at 6961.9 eV (Figure 6). All three states represent transitions to minority-spin ( $\beta$ ) levels. For Fe[TPC]Ph, two dominant transitions (States 4 and 5) were found. State 4 at

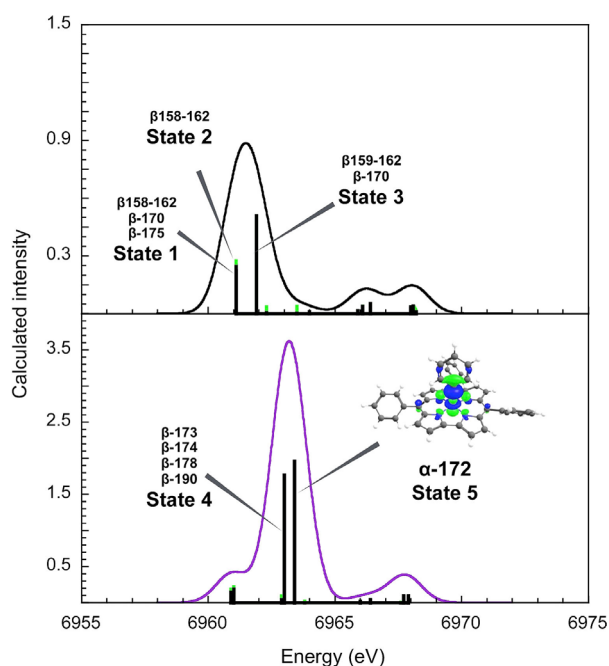


**Figure 6.** Individual transitions contributing to the TDDFT  $1s \rightarrow 3d$  spectra of Fe[TPC]Cl (top) and Fe[TPC]Ph (bottom). Dipole and quadrupole contributions are indicated in black and green, respectively.

6962.6 eV involves transitions to  $\beta$  levels, whereas State 5, at 6963 eV, is attributed solely to a  $1s \rightarrow \alpha$ -172 (LUMO) transition. State 5 contributes around 41% to the calculated pre-edge intensity and accounts for much of the observed increase in Fe K pre-edge intensity for Fe[TPC]Ph relative to Fe[TPC]Cl. In other words, the extra Fe $3d_{z^2}$ -based hole, with significant symmetry-allowed  $4p_z$  character, accounts for the greatly enhanced pre-edge intensity of Fe[TPC]Ph. The fact that the additional hole is Fe $3d_{z^2}$ -based is directly responsible for the dramatic difference in the Fe K pre-edges, which makes the method extremely sensitive for determining metal- versus ligand-based oxidation.

The above results constitute some of the first evidence that a combined Fe K-edge XANES and theoretical approach may be used successfully to probe the question of ligand noninnocence in metallocorroles. An interesting question concerns whether the relatively high pre-edge intensity observed for  $\{\text{Fe}[\text{TPC}]\}_2\text{O}$  might signify higher Fe $^{\text{IV}}$  character relative to the FeCl and FeNO complexes. The short Fe–O distances in  $\{\text{Fe}[\text{TPC}]\}_2\text{O}$  are expected to result in increased  $3d_{z^2}$ – $4p_z$  mixing, and hence, increased pre-edge intensity. This effect has also been noted elsewhere by Neese, DeBeer, and co-workers.<sup>[26]</sup> Unfortunately, given the large molecular size of  $\{\text{Fe}[\text{TPC}]\}_2\text{O}$  and the complex four-center antiferromagnetic coupling, a satisfactory TDDFT analysis of this compound has so far proved unfeasible. The question of higher Fe $^{\text{IV}}$  character in this compound thus remains unsettled, even though it dovetails with the lower Soret shifts observed for the  $\{\text{Fe}[\text{TpXPC}]\}_2\text{O}$  series.

### Redox potentials as a potential probe of ligand noninnocence

The simplicity of the optical probe described above led us to consider whether the redox potentials of metallocorroles might offer similar clues as to the innocent/noninnocent character of the corrole macrocycle. Metallocorroles with redox-inactive metal centers such as ReO, OsN, and Au exhibit large electrochemical HOMO–LUMO gaps of around 2.2 V, which is essentially the  $\pi$ – $\pi^*$  gap of an innocent corrole ligand.<sup>[21,27]</sup> In contrast, the electrochemical HOMO–LUMO gaps of iron corroles are less than half that value, that is, approximately 1.0 V (Figure 7 and Table 3). In this regard, they resemble the noninnocent copper corroles. Furthermore, note that the innocent FePh and FeTol corrole $^{3-}$  series and the noninnocent FeCl, FeNO, and Fe $_2(\mu\text{-O})$  corrole $^{2-}$  series do not exhibit distinctly different electrochemical HOMO–LUMO gaps, nor are there major differences in the first oxidation or reduction potentials between the different classes (i.e., innocent/noninnocent) of iron corroles. The surprising invariance of redox potentials across innocent and noninnocent Fe corroles is best viewed as a coincidence: the reduction of FePh and FeCl corroles involves different chemical processes, namely the addition of an electron to Fe $^{\text{IV}}$  and to a corrole $^{2-}$  radical, respectively, but the final, reduced state is similar in both cases, that is, Fe $^{\text{III}}$ -corrole $^{3-}$ . We are thus led to conclude that the redox potentials of metallocorroles with redox-active metal centers do not, by

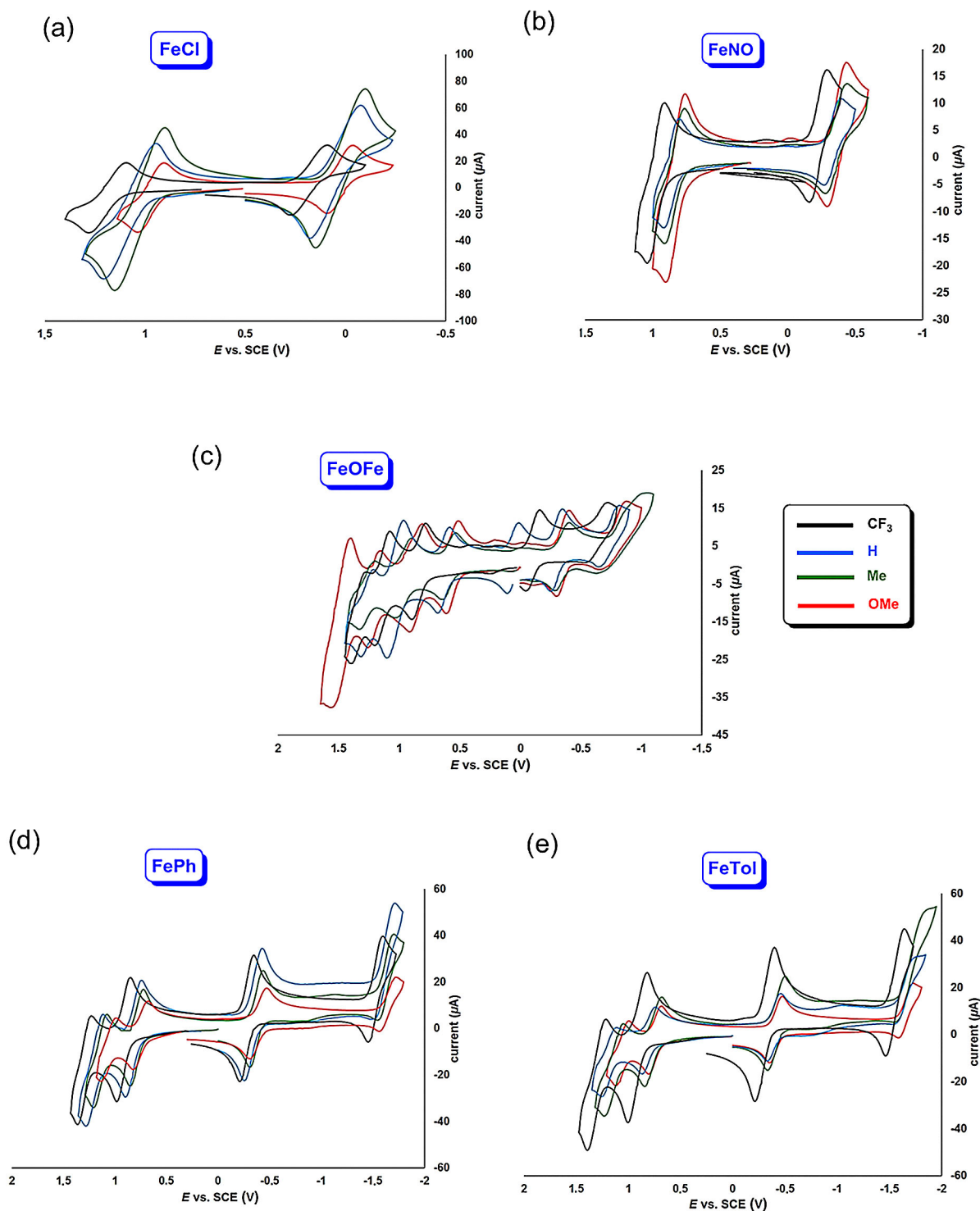


Figure 7. Cyclic voltammograms (V vs. SCE) for the iron corroles studied.

themselves, indicate the innocence or noninnocence of the corrole ligand.

## Conclusions

The present study was undertaken not so much to derive new insight into the electronic structures of Fe corroles, which we

have understood qualitatively for some time, but rather, to validate key experimental approaches as probes of ligand noninnocence. Our main conclusions may be summarized as follows.

1. The Soret maxima of the FePh and FeTol series were found to be insensitive to the *para* substituent X, consistent with the presumed innocence of the corrole ligand in these compounds. Although not surprising, this finding significantly

**Table 3.** Electrochemical data (V) for the compounds studied.

Series	X	$E_{ox4}$	$E_{ox3}$	$E_{ox2}$	$E_{ox1}$	$E_{red1}$	$E_{red2}$	$E_{HOMO-LUMO}$
Fe[TpXPC]Cl <sup>[a]</sup>	CF <sub>3</sub>	–	–	–	1.18	0.19	–	0.99
	H	–	–	–	1.09	0.04	–	1.05
	Me	–	–	–	1.05	0.00	–	1.05
	OMe	–	–	–	0.97	0.03	–	0.94
Fe[TpXPC](NO) <sup>[b]</sup>	CF <sub>3</sub>	–	–	–	0.98	–0.22	–	1.20
	H	–	–	–	0.86	–0.33	–	1.19
	Me	–	–	–	0.84	–0.36	–	1.20
	OMe	–	–	–	0.83	–0.37	–	1.20
{Fe[TpXPC]} <sub>2</sub> O	CF <sub>3</sub>	–	1.33	1.14	0.84	–0.10	–0.63	0.94
	H	–	1.26	1.03	0.63	–0.30	–0.73	0.93
	Me	–	1.27	0.96	0.59	–0.34	–0.76	0.93
	OMe	1.48	1.21	0.86	0.56	–0.35	–0.77	0.91
Fe[TpXPC]Ph	CF <sub>3</sub>	–	–	1.29	0.92	–0.27	–1.52	1.19
	H	–	–	1.20	0.82	–0.35	–1.62	1.17
	Me	–	–	1.14	0.78	–0.37	–1.63	1.15
	OMe	–	–	1.09	0.76	–0.39	–1.67	1.15
Fe[TpXPC]Tol	CF <sub>3</sub>	–	–	1.30	0.91	–0.30	–1.57	1.21
	H	–	–	1.17	0.80	–0.40	–1.66	1.20
	Me	–	–	1.14	0.77	–0.42	–1.72	1.19
	OMe	–	–	1.06	0.74	–0.41	–1.65	1.15
Cu[TpXPC] <sup>[c]</sup>	CF <sub>3</sub>	–	–	–	0.89	–0.08	–	0.97
	H	–	–	–	0.76	–0.20	–	0.96
	Me	–	–	–	0.70	–0.23	–	0.93
	OMe	–	–	–	0.65	–0.24	–	0.89
Au[TpXPC] <sup>[d]</sup>	CF <sub>3</sub>	–	–	–	0.94	–1.29	–	2.23
	H	–	–	1.35	0.80	–1.38	–	2.18
	Me	–	–	1.35	0.78	–1.42	–	2.20
	OMe	–	–	1.32	0.76	–1.57	–	2.33

[a] Refs [4] and [12]. [b] Ref [11a]. [c] Ref [3a]. [d] Ref [10c].

boosts our confidence in Soret substituent effects as a probe of corrole noninnocence.

2. Fe K-edge XANES was used for the first time to address the question of ligand noninnocence in Fe corroles. Four representative Fe corroles, namely, Fe[TPC]Cl, Fe[TPC](NO), {Fe[TPC]}<sub>2</sub>O, and Fe[TPC]Ph, were selected for this purpose. Although the complexes were found to exhibit only modest variations in intensity weighted average energy (IWAE) positions, the integrated pre-edge intensities were found to vary considerably: Fe[TPC]Cl (1.37) < Fe[TPC](NO) (1.55) < [{Fe[TPC]}<sub>2</sub>O] (3.02) < Fe[TPC]Ph (3.61). In the context of the similar ligand systems and geometries, the significant increase in pre-edge intensity in Fe[TPC]Ph was found to be indicative of a higher number of 3d holes, consistent with an Fe<sup>IV</sup>-like description, whereas the lower pre-edge intensities of Fe[TPC]Cl and Fe[TPC]NO are consistent with an Fe<sup>III</sup>-like description. The results provide strong validation of XANES as a probe of ligand noninnocence in Fe corroles and, by extension, to metallocorroles in general.

3. We were interested in determining whether electrochemical redox potentials might afford a simple probe of ligand noninnocence, akin to the simple optical probe. The answer to this question is “no”: the first oxidation and reduction potentials and the electrochemical HOMO–LUMO gaps are all remarkably similar across the various Fe corrole families examined.

## Experimental Section

### Materials

Free-base corroles H<sub>3</sub>[TpXPC],<sup>[28]</sup> Fe-corrole diethyl ether complexes Fe[TpXPC](Et<sub>2</sub>O)<sub>2</sub>,<sup>[29]</sup> and FeCl corroles Fe[TpXPC]Cl<sup>[4]</sup> (in which X = CF<sub>3</sub>, H, CH<sub>3</sub>, and OCH<sub>3</sub>) were synthesized as described previously. The synthetic protocol for Fe-aryl corroles was also adapted from the literature.<sup>[30]</sup> Silica gel 150 (35–70 μm particle size, Davisil) was used for flash chromatography. Silica gel 60 preparative thin-layer chromatographic (PLC) plates (20 cm × 20 cm × 0.5 mm, Merck) were used for the final purification of the new complexes.

### Instrumentation

UV/Vis spectra were recorded on an HP 8453 spectrophotometer with dry dichloromethane as the solvent. Cyclic voltammetry was performed with an EG&G Model 263A potentiostat equipped with a three-electrode system, consisting of a glassy carbon working electrode, a platinum wire counter electrode, and a saturated calomel reference electrode (SCE). Tetra(*n*-butyl)ammonium perchlorate (TBAP), recrystallized three times from absolute ethanol and dried in a desiccator for at least two weeks, was used as the supporting electrolyte. The reference electrode was separated from the bulk solution by a fritted-glass bridge filled with the solvent/supporting electrolyte mixture. All potentials were referenced to the SCE. The anhydrous dichloromethane solutions were purged with argon for at least 5 min prior to the measurements, and an argon blanket was maintained over the solutions during the measurements. <sup>1</sup>H (400 MHz) and <sup>19</sup>F (376 MHz) NMR spectra were recorded in CDCl<sub>3</sub> on a Mercury Plus Varian spectrometer and referenced to residual CHCl<sub>3</sub> (7.26 ppm) and to 2,2,2-trifluoroethanol-*d*<sub>3</sub> (δ = –77.8 ppm), respectively. High-resolution electrospray ionization (HR-ESI) mass spectra were recorded on an LTQ Orbitrap XL spectrometer.

### Synthesis of Fe-aryl corroles

A detailed procedure is described below for the synthesis of Fe[TPC]Ph. The same essential procedure was also applicable to the other Fe-aryl corroles. The optimum methods for chromatographic purification, however, are different for the various new iron complexes, and are indicated below.

**Synthesis of Fe[TPC]Ph:** Fe[TPC]Cl (40 mg, 0.065 mmol) was introduced into a 50 mL one-necked round-bottomed flask equipped with a magnetic stirring bar. Anhydrous CH<sub>2</sub>Cl<sub>2</sub> (12 mL) was added with a syringe under argon and the mixture was stirred under argon for 3–4 min. Phenylmagnesium bromide (5 equiv., 3.0 M in diethyl ether) was then added with a syringe, and the mixture was stirred under argon for 10 min, during which the solution turned from yellow–brown to dark red. The solution was then quenched with an excess of distilled water and extracted with dichloromethane. The organic fraction was dried with anhydrous Na<sub>2</sub>SO<sub>4</sub> and filtered, and the filtrate was dried on a rotary evaporator. The dark brown residue obtained was purified by silica gel column chromatography with 4:1 *n*-hexane/CH<sub>2</sub>Cl<sub>2</sub> as eluent. The Fe[TPC]Ph eluted as an intense dark red band, which was collected and evaporated to dryness. The product was further purified by preparative thin layer chromatography (PLC) with 3:1 *n*-hexane/CH<sub>2</sub>Cl<sub>2</sub> as eluent. The pure product eluted as the first red band (17.5 mg, 41%). UV/Vis (CH<sub>2</sub>Cl<sub>2</sub>) λ<sub>max</sub> (ε × 10<sup>–4</sup>) = 383 (4.94), 505 (0.97), 646 nm (0.24 M<sup>–1</sup> cm<sup>–1</sup>); <sup>1</sup>H NMR: δ = 14.84, 13.79 (bs, 4H, 5,15-*o*), 11.98, 11.83 (bs, 2H, 10-*o*), 10.95 (bs, 2H, 7,13-β), 10.86 (s, 2H, 5,15-*p*), 9.65 (s, 1H, 10-*p*), 6.26, 6.02 (s, 4H, 5,15-*m*), 5.72, 5.60 (s, 2H, 10-*m*), –0.51 (bs, 2H, *m*, axial Ph), –30.90 (bs, 2H, 2,18-β), –56.74 (bs, 2H,



8,12- $\beta$ ), -87.41 (bs, 1H, *p*, axial Ph), -109.66 (bs, 2H, 3,17- $\beta$ ), -155.89 ppm (bs, 2H, *o*, axial Ph); HRMS (ESI<sup>+</sup>, major isotopomer): *m/z* calcd for [M]<sup>+</sup>: 656.1658; found: 656.1649; elemental analysis calcd (%): C 78.66, H 4.30, N 8.53; found: C 77.85, H 4.81, N 8.22.

**Purification of Fe[TPC]Tol:** Silica gel column chromatography was performed with 4:1 *n*-hexane/CH<sub>2</sub>Cl<sub>2</sub> as eluent, followed by PLC with 3:1 *n*-hexane/CH<sub>2</sub>Cl<sub>2</sub> as eluent. Pure Fe[TPC]Tol eluted as the first red band (17 mg, 39%). UV/Vis (CH<sub>2</sub>Cl<sub>2</sub>):  $\lambda_{\max}$  ( $\epsilon \times 10^{-4}$ ) = 385 (5.0), 503 (0.92), 645 nm (0.23 M<sup>-1</sup> cm<sup>-1</sup>); <sup>1</sup>H NMR:  $\delta$  = 14.73, 13.70 (bs, 4H, 5,15-*o*), 11.94, 11.77 (bs, 2H, 10-*o*), 10.81 (s, 2H, *s*, 5,15-*p*), 10.71 (bs, 2H, 7,13- $\beta$ ); 9.62 (s, 1H, 10-*p*), 6.27, 6.04 (s, 4H, 5,15-*m*), 5.77, 5.64 (s, 2H, 10-*m*), 2.89 (bs, 2H, *m*, axial Tol), -30.0 (bs, 2H, 2,18- $\beta$ ), -55.26 (bs, 2H, 8,12- $\beta$ ), -107.22 (bs, 3H, *p*Me, axial Tol), -152.46 (bs, 2H, 3,17- $\beta$ ), -158.69 ppm (bs, 2H, *o*, axial Tol); HRMS (ESI<sup>+</sup>, major isotopomer): *m/z* calcd for [M]<sup>+</sup>: 670.1815; found: 670.1823; elemental analysis calcd (%): C 78.81, H 4.51, N 8.35; found: C 77.63, H 4.95, N 8.02.

**Purification of Fe[TpMePC]Tol:** Silica gel column chromatography was performed with 3:1 *n*-hexane/CH<sub>2</sub>Cl<sub>2</sub> as eluent, followed by PLC with 3:1 *n*-hexane/CH<sub>2</sub>Cl<sub>2</sub> as eluent. Pure Fe[TpMePC]Tol eluted as the first red band (15 mg, 35%). UV/Vis (CH<sub>2</sub>Cl<sub>2</sub>):  $\lambda_{\max}$  ( $\epsilon \times 10^{-4}$ ) = 383 (6.29), 505 (1.13), 646 nm (0.20 M<sup>-1</sup> cm<sup>-1</sup>); <sup>1</sup>H NMR:  $\delta$  = 14.75, 13.70 (bs, 4H, 5,15-*o*), 12.0, 11.79 (bs, 2H, 10-*o*), 10.30 (bs, 2H, 7,13- $\beta$ ); 5.97, 5.73 (s, 4H, 5,15-*m*), 5.41, 5.27 (s, 2H, 10-*m*), 3.58 (bs, 2H, *m*, axial Tol), 0.82 (s, 3H, 10-*p*Me), 0.62 (s, 6H, 5,15-*p*Me), -29.97 (bs, 2H, 2,18- $\beta$ ), -54.57 (bs, 2H, 8,12- $\beta$ ), -106.93 (bs, 3H, *p*Me, axial Tol), -156.81 (bs, 2H, 3,17- $\beta$ ), -162.99 ppm (bs, 2H, *o*, axial Tol); HRMS (ESI<sup>+</sup>, major isotopomer): *m/z* calcd for [M]<sup>+</sup>: 712.2285; found: 712.2294; elemental analysis calcd (%): C 79.21, H 5.09, N 7.86; found: C 78.36, H 5.50, N 7.58.

**Purification of Fe[TpOMePC]Ph:** Silica gel column chromatography was performed with 2:3 *n*-hexane/CH<sub>2</sub>Cl<sub>2</sub> as eluent, followed by PLC with the same solvent mixture as eluent. Pure Fe[TpOMePC]Ph eluted as the first red band (12 mg, 28%). UV/Vis (CH<sub>2</sub>Cl<sub>2</sub>):  $\lambda_{\max}$  ( $\epsilon \times 10^{-4}$ ) = 385 (5.18), 505 (0.84), 542 (0.71), 645 nm (0.1 M<sup>-1</sup> cm<sup>-1</sup>); <sup>1</sup>H NMR:  $\delta$  = 14.89, 13.81 (bs, 4H, 5,15-*o*), 12.17, 11.97 (bs, 2H, 10-*o*), 10.23 (bs, 2H, 7,13- $\beta$ ), 5.88, 5.61 (s, 4H, 5,15-*m*), 5.22, 5.07 (s, 2H, 10-*m*), 4.17 (s, 6H, 5,15-*p*OMe), 3.92 (s, 3H, 10-*p*OMe), 0.66 (bs, 2H, *m*, axial Ph), -30.73 (bs, 2H, 2,18- $\beta$ ), -55.23 (bs, 2H, 8,12- $\beta$ ), -86.48 (bs, 1H, *p*, axial Ph), -108.98 (bs, 2H, 3,17- $\beta$ ), -153.07 ppm (bs, 2H, *o*, axial Ph); HRMS (ESI<sup>-</sup>, major isotopomer): *m/z* calcd for [M]<sup>-</sup>: 746.1987; found: 746.1963; elemental analysis calcd (%): C 73.51, H 4.90, N 7.50; found: C 73.99, H 4.59, N 7.34.

**Purification of Fe[TpOMePC]Tol:** Silica gel column chromatography was performed with 1:1 *n*-hexane/CH<sub>2</sub>Cl<sub>2</sub> as eluent, followed by PLC with 2:3 *n*-hexane/CH<sub>2</sub>Cl<sub>2</sub> as eluent. Pure Fe[TpOMePC]Tol eluted as the first red band (15 mg, 35%). UV/Vis (CH<sub>2</sub>Cl<sub>2</sub>):  $\lambda_{\max}$  ( $\epsilon \times 10^{-4}$ ) = 386 (7.57), 505 (1.22), 547 (1.14), 645 nm (0.21 M<sup>-1</sup> cm<sup>-1</sup>); <sup>1</sup>H NMR:  $\delta$  = 14.82, 13.72 (bs, 4H, 5,15-*o*, *p*OMeP), 12.13, 11.91 (bs, 2H, 10-*o*, *p*OMeP), 10.02 (bs, 2H, 7,13- $\beta$ ), 5.89, 5.62 (s, 4H, 5,15-*m*, *p*OMeP), 5.30, 5.11 (s, 2H, 10-*m*, *p*OMeP), 4.17 (s, 6H, 5,15-*p*OMe), 3.93 (s, 3H, 10-*p*OMe), -29.87 (bs, 2H, 2,18- $\beta$ ), -53.83 (bs, 2H, 8,12- $\beta$ ), -106.58 (bs, 3H, *p*Me,  $\sigma$ -Tolyl), -118.06 (bs, 2H, 3,17- $\beta$ ), -155.61 ppm (bs, 2H, *o*,  $\sigma$ -Tolyl). The *meta* protons of the axial Tol could not be located, presumably owing to peak broadening. HRMS (ESI<sup>-</sup>, major isotopomer): *m/z* calcd for [M]<sup>-</sup>: 760.2143; found: 760.2120; elemental analysis calcd (%): C 74.21, H 4.77, N 7.37; found: C 72.86, H 4.97, N 7.06.

**Purification of Fe[TpCF<sub>3</sub>PC]Ph:** Silica gel column chromatography was performed with 7:3 *n*-hexane/CH<sub>2</sub>Cl<sub>2</sub> as eluent, followed by PLC with the same solvent mixture as eluent. Pure Fe[TpCF<sub>3</sub>PC]Ph eluted as the first red band (15 mg, 36%). UV/Vis (CH<sub>2</sub>Cl<sub>2</sub>):  $\lambda_{\max}$  ( $\epsilon \times$

$10^{-4}$ ) = 384 (6.91), 503 (1.07), 542 nm (0.96 M<sup>-1</sup> cm<sup>-1</sup>); <sup>1</sup>H NMR:  $\delta$  = 14.59, 13.56 (bs, 4H, 5,15-*o*), 12.08–11.50 (overlapping bs, 4H, 10-*o* and 7,13- $\beta$ ), 6.66, 6.43 (s, 4H, 5,15-*m*), 6.18, 6.07 (s, 2H, 10-*m*), -3.41 (bs, 2H, *m*, axial Ph), -31.15 (bs, 2H, 2,18- $\beta$ ), -59.05 (bs, 2H, 8,12- $\beta$ ), -89.80 (bs, 1H, *p*, axial Ph), -110.60 (bs, 2H, 3,17- $\beta$ ), -163.10 ppm (bs, 2H, *o*, axial Ph); <sup>19</sup>F NMR:  $\delta$  = -64.90 (s, 3F), -65.29 ppm (s, 6F); HRMS (ESI<sup>-</sup>, major isotopomer): *m/z* calcd for [M]<sup>-</sup>: 860.1291; found: 860.1282; elemental analysis calcd (%): C 64.20, H 2.93, N 6.51; found: C 63.66, H 3.50, N 6.26.

**Purification of Fe[TpCF<sub>3</sub>PC]Tol:** Silica gel column chromatography was performed with 7:3 *n*-hexane/CH<sub>2</sub>Cl<sub>2</sub> as eluent, followed by PLC with 3:1 *n*-hexane/CH<sub>2</sub>Cl<sub>2</sub> as eluent. Pure Fe[TpCF<sub>3</sub>PC]Tol eluted as the first red band (27 mg, 63%). UV/Vis (CH<sub>2</sub>Cl<sub>2</sub>):  $\lambda_{\max}$  ( $\epsilon \times 10^{-4}$ ) = 387 (7.00), 505 (1.13), 544 (1.11), 640 nm (0.17 M<sup>-1</sup> cm<sup>-1</sup>); <sup>1</sup>H NMR:  $\delta$  = 14.51, 13.45 (bs, 4H, 5,15-*o*), 12.01–11.19 (overlapping bs, 4H, 10-*o* and 7,13- $\beta$ ), 6.69, 6.45 (s, 4H, 5,15-*m*), 6.25, 6.14 (s, 2H, 10-*m*), 0.25 (bs, 2H, *m*, axial Tol), -30.24 (bs, 2H, 2,18- $\beta$ ), -57.33 (bs, 2H, 8,12- $\beta$ ), -107.72 (bs, 3H, *p*Me, axial Tol), -114.20 (bs, 2H, 3,17- $\beta$ ), -165.23 ppm (bs, 2H, *o*, axial Tol); <sup>19</sup>F NMR:  $\delta$  = -64.85 (s, 3F), -65.24 (s, 6F); HRMS (ESI<sup>-</sup>, major isotopomer): *m/z* calcd for [M]<sup>-</sup>: 874.1448; found: 874.1440; elemental analysis calcd (%): C 64.54, H 3.11, N 6.40; found: C 64.80, H 3.28, N 6.16.

### X-ray absorption measurement and analysis

The Fe K-edge X-ray absorption spectra of Fe[TPC]Cl, Fe[TPC](NO), {Fe[TPC]}<sub>2</sub>O, and Fe[TPC]Ph were collected at the Stanford Synchrotron Radiation Lightsource under standard ring conditions of 3 GeV and  $\approx$  500 mA on the unfocused 20-pole 2 T wiggler side-station 7-3, equipped with a Si(220) double crystal monochromator for energy selection. The M0 mirror was not employed and the monochromator was detuned by  $\approx$  50% to eliminate contributions from higher harmonics. All complexes were measured as solutions ( $\approx$  10 mM in Fe, prepared in benzene). Delrin XAS cells (2 mm) wrapped in Kapton tape were used, and the solution sample cells were stored under liquid N<sub>2</sub>. During the data collection, the samples were maintained at a constant temperature of  $\approx$  10–15 K using an Oxford liquid He cryostat. Fe K-edge EXAFS data were measured to  $k = 16 \text{ \AA}^{-1}$  (fluorescence mode) using a Canberra Ge 30-element array detector. Internal energy calibration was accomplished by simultaneous measurement of the absorption of an Fe foil placed between the second and third ionization chambers situated after the sample. The data were calibrated to the first inflection point of the Fe foil (7111.2 eV). At least two sweeps were collected to ensure that no radiation damage was observed. The energy calibration, background correction, data averaging, and normalization were accomplished with ATHENA,<sup>[31]</sup> which is part of the Demeter software package version 0.9.24. The pre-edge regions of the data sets were fit using Peak-Fit (SigmaPlot).

### Theoretical calculations

All DFT calculations were performed with the B3LYP functional and a spin-unrestricted formalism, allowing for broken-symmetry solutions, using the ORCA 3.0.3 program system.<sup>[32]</sup> In general, we used Ahlrich's all-electron triple- $\zeta$  triple polarization basis set TZVPPP for Fe and TZVPP for all other atoms.<sup>[33]</sup> The calculations on {Fe[TPC]}<sub>2</sub>O, however, could only be performed with the smaller def-2 basis set. Furthermore, all calculations were performed in a dielectric continuum using the conductor-like screening model (COSMO)<sup>[34]</sup> with a dielectric constant of 4, and tight SCF convergence criteria were employed throughout. The SlowConv criterion was employed. An SCF grid of 4 with no finalgrid was used. A higher grid (grid7) was used on the Fe atom. For broken-symmetry

calculations, the BrokenSym keyword was employed. TDDFT calculations (as implemented in the ORCA package) were employed to calculate the energies and intensities of the Fe K pre-edges. The number of roots was set at 20, MaxDim was set at 200, "doQuad True" was selected, and triplets were not calculated. The TDDFT calculations were performed over the entire valence manifold and for both the spin-up and spin-down transitions. The calculated energies and intensities were broadened with the Peak-Fit (Sigma-Plot, Systat Software) Gaussian-Lorentzian sum function with half-widths of 1.5 eV to account for core-hole lifetime and instrument broadening. The calculated pre-edge energies were linearly up-shifted by 151 eV for comparison with the experimental spectra.

## Acknowledgements

This work was supported by projects 231086 and 262229 of the Research Council of Norway (AG) and the SSRL Structural Molecular Biology (SMB) resource. The SSRL SMB is supported by the NIH National Institute of General Medical Sciences (NIGMS) through a Biomedical Technology Research Resource P41 grant (P41GM103393) and by the DOE Office of Biological and Environmental Research. LJG was supported by a postdoctoral fellowship from Stanford University.

## Conflict of interest

The authors declare no conflict of interest.

**Keywords:** corroles · iron · noninnocence · XANES · X-ray absorption spectroscopy

- [1] A. Ghosh, *Chem. Rev.* **2017**, *117*, 3798–3881.
- [2] a) A. Ghosh, E. Steene, *J. Inorg. Biochem.* **2002**, *91*, 423–436; b) H.-Y. Liu, M. H. R. Mahmood, S. X. Qiuc, C. K. Chang, *Coord. Chem. Rev.* **2013**, *257*, 1306–1333.
- [3] a) I. H. Wasbotten, T. Wondimagegn, A. Ghosh, *J. Am. Chem. Soc.* **2002**, *124*, 8104–8116; b) C. Brückner, R. P. Briñas, J. A. K. Bauer, *Inorg. Chem.* **2003**, *42*, 4495–4497; c) Z. Ou, J. Shao, H. Zhao, K. Ohkubo, I. H. Wasbotten, S. Fukuzumi, A. Ghosh, K. M. Kadish, *J. Porphyrins Phthalocyanines* **2004**, *8*, 1236–1247; d) M. Bröring, F. Brégier, E. C. Tejero, C. Hell, M. C. Holthausen, *Angew. Chem. Int. Ed.* **2007**, *46*, 445–448; *Angew. Chem.* **2007**, *119*, 449–452; e) A. B. Alemayehu, E. Gonzalez, L.-K. Hansen, A. Ghosh, *Inorg. Chem.* **2009**, *48*, 7794–7799; f) A. B. Alemayehu, L.-K. Hansen, A. Ghosh, *Inorg. Chem.* **2010**, *49*, 7608–7610; g) S. Berg, K. E. Thomas, C. M. Beavers, A. Ghosh, *Inorg. Chem.* **2012**, *51*, 9911–9916; h) K. E. Thomas, H. Vazquez-Lima, Y. Fang, Y. Song, K. J. Gagnon, C. M. Beavers, K. M. Kadish, A. Ghosh, *Chem. Eur. J.* **2015**, *21*, 16839–16847.
- [4] E. Steene, T. Wondimagegn, A. Ghosh, *J. Phys. Chem. B* **2001**, *105*, 11406–11413; addition/correction: E. Steene, T. Wondimagegn, A. Ghosh, *J. Phys. Chem. B* **2002**, *106*, 5312–5312.
- [5] O. Zakharieva, V. Schünemann, M. Gerdan, S. Licocchia, S. Cai, F. A. Walker, A. X. Trautwein, *J. Am. Chem. Soc.* **2002**, *124*, 6636–6648.
- [6] F. A. Walker, S. Licocchia, R. Paolesse, *J. Inorg. Biochem.* **2006**, *100*, 810–837.
- [7] For a DFT study of potential Fe<sup>V</sup> corroles, see: I. Wasbotten, A. Ghosh, *Inorg. Chem.* **2006**, *45*, 4910–4913.
- [8] Iron corroles in which the axial ligand is intermediate in ligand field strength compared with Cl and Ph have not yet been reported.
- [9] A. B. Alemayehu, H. Vazquez-Lima, C. M. Beavers, K. J. Gagnon, J. Bendix, A. Ghosh, *Chem. Commun.* **2014**, *50*, 11093–11096.
- [10] a) A. B. Alemayehu, A. Ghosh, *J. Porphyrins Phthalocyanines* **2011**, *15*, 106–110; b) E. Rabinovich, I. Goldberg, Z. Gross, *Chem. Eur. J.* **2011**, *17*, 12294–12301; c) K. E. Thomas, A. B. Alemayehu, J. B. Conradie, C. M. Beavers, A. Ghosh, *Inorg. Chem.* **2011**, *50*, 12844–12851; d) K. E. Thomas, C. M. Beavers, A. Ghosh, *Mol. Phys.* **2012**, *110*, 2439–2444.
- [11] a) H. Vazquez-Lima, H.-K. Norheim, A. R. F. Einrem, A. Ghosh, *Dalton Trans.* **2015**, *44*, 10146–10151; b) H.-K. Norheim, J. Capar, R. F. Einrem, K. J. Gagnon, C. M. Beavers, H. Vazquez-Lima, A. Ghosh, *Dalton Trans.* **2016**, *45*, 681–689.
- [12] S. Ganguly, H. Vazquez-Lima, A. Ghosh, *Chem. Eur. J.* **2016**, *22*, 10336–10340.
- [13] A. B. Alemayehu, J. Conradie, A. Ghosh, *Eur. J. Inorg. Chem.* **2011**, 1857–1864.
- [14] Thus, noninnocent metallocorroles may be said to exhibit hyper spectra: I. H. Wasbotten, J. Conradie, A. Ghosh, *J. Phys. Chem. B* **2003**, *107*, 3613–3623.
- [15] I. Johansen, H.-K. Norheim, S. Larsen, A. B. Alemayehu, J. Conradie, A. Ghosh, *J. Porphyrins Phthalocyanines* **2011**, *15*, 1335–1344.
- [16] A. B. Alemayehu, K. J. Gagnon, J. Turner, A. Ghosh, *Angew. Chem. Int. Ed.* **2014**, *53*, 14411–14414; *Angew. Chem.* **2014**, *126*, 14639–14642.
- [17] R. F. Einrem, K. J. Gagnon, A. B. Alemayehu, A. Ghosh, *Chem. Eur. J.* **2016**, *22*, 517–520.
- [18] R. F. Einrem, H. Braband, T. Fox, H. Vazquez-Lima, R. Alberto, A. Ghosh, *Chem. Eur. J.* **2016**, *22*, 18747–18751.
- [19] a) F. de Groot, *Chem. Rev.* **2001**, *101*, 1779–1808; b) R. Sarangi, *Coord. Chem. Rev.* **2013**, *257*, 459–472.
- [20] a) R. K. Hocking, S. D. George, Z. Gross, F. A. Walker, K. O. Hodgson, B. Hedman, E. I. Solomon, *Inorg. Chem.* **2009**, *48*, 1678–1688; b) R. Sarangi, L. J. Giles, K. E. Thomas, A. Ghosh, *Eur. J. Inorg. Chem.* **2016**, 3225–3227.
- [21] Y. Fang, Z. Ou, K. M. Kadish, *Chem. Rev. Art. ASAP*: <http://pubs.acs.org/doi/abs/10.1021/acs.chemrev.6b00546>.
- [22] Unfortunately, this question is experimentally rather intractable. Unlike S=1 FeCl and Fe-aryl corroles, FeNO and μ-oxo diiron corroles are diamagnetic, and thus, afford no direct NMR or EPR probe of radical character. X-ray crystallography has revealed characteristic and comparable skeletal bond length alternations for FeCl, FeNO, and μ-oxo diiron corroles, which are indicative of corrole radical character. On the other hand, broken-symmetry DFT calculations have indicated stronger Fe<sup>III</sup>(S=3/2)-corrole<sup>2-</sup> antiferromagnetic coupling for μ-oxo diiron corroles than for FeCl and FeNO corroles, consistent with a lesser degree of radical character in the former complexes, as proposed here.<sup>[12]</sup>
- [23] For an earlier, pertinent DFT study, see: B. Van Oort, E. Tangen, A. Ghosh, *Eur. J. Inorg. Chem.* **2004**, 2442–2445.
- [24] For a recent study of Fe[TpMePC]Ph, see: S. Nardis, D. O. Cicero, S. Licocchia, G. Pomarico, B. B. Berna, M. Sette, G. Ricciardi, A. Rosa, F. R. Fronczek, K. M. Smith, R. Paolesse, *Inorg. Chem.* **2014**, *53*, 4215–4227.
- [25] B. O. Roos, V. Veryazov, J. Conradie, P. R. Taylor, A. Ghosh, *J. Phys. Chem. B* **2008**, *112*, 14099–14102.
- [26] P. Chandrasekaran, S. C. E. Stieber, T. J. Collins, L. Que, Jr., F. Neese, S. DeBeer, *Dalton Trans.* **2011**, *40*, 11070–11079.
- [27] For electrochemical HOMO–LUMO gaps of closed-shell corrole derivatives, see: L. Simkhovich, A. Mahammed, I. Goldberg, Z. Gross, *Chem. Eur. J.* **2001**, *7*, 1041–1055.
- [28] B. Koszarna, T. D. Gryko, *J. Org. Chem.* **2006**, *71*, 3707–3717.
- [29] L. Simkhovich, I. Goldberg, Z. Gross, *Inorg. Chem.* **2002**, *41*, 5433–5439.
- [30] E. Vogel, S. Will, A. S. Tilling, L. Neumann, J. Lex, E. Bill, A. X. Trautwein, K. Wieghardt, *Angew. Chem. Int. Ed. Engl.* **1994**, *33*, 731–735; *Angew. Chem.* **1994**, *106*, 771–775.
- [31] B. Ravel, M. Newville, *J. Synchrotron Radiat.* **2005**, *12*, 537–541.
- [32] a) F. Neese, G. Olbrich, *Chem. Phys. Lett.* **2002**, *362*, 170–178; b) Neese, F. ORCA, An ab initio, DFT and semiempirical SCF-MO package, Version 3.0.3, University of Bonn, Germany, **2016**.
- [33] F. Weigend, R. Ahlrichs, *Phys. Chem. Chem. Phys.* **2005**, *7*, 3297–3305.
- [34] S. Sinnecker, A. Rajendran, A. Klamt, M. Diedenhofen, F. Neese, *J. Phys. Chem. A* **2006**, *110*, 2235–2245.

Manuscript received: June 7, 2017

Accepted manuscript online: August 28, 2017

Version of record online: ■■■■■ 0000

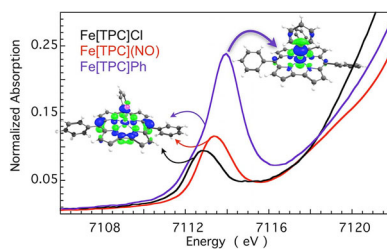
## FULL PAPER

### Ligand Noninnocence

S. Ganguly, L. J. Giles, K. E. Thomas,  
R. Sarangi,\* A. Ghosh\*



**Ligand Noninnocence in Iron Corroles:  
Insights from Optical and X-ray  
Absorption Spectroscopies and  
Electrochemical Redox Potentials**



**Probing ligand noninnocence:** Like optical spectroscopy, X-ray absorption near-edge spectroscopy (XANES) provides an excellent probe of ligand noninnocence in iron corroles. Electrochemical redox potentials, on the other hand, do not correlate straightforwardly with ligand noninnocence.